Research Square

Preprints are preliminary reports that have not undergone peer review.
They should not be considered conclusive, used to inform clinical practice,
or referenced by the media as validated information.

# Bleomycin as an Inducer of Senescence in RAW 264.7 Macrophages

**Kamand Kavianpour**
University of Tübingen
**Oliver Hihn**
University of Tübingen
**Marijana Baotic**
University of Tübingen
**Bettina Weigelin**
University of Tübingen
**Bernd Pichler**
University of Tübingen
**Nicolas Beziere**
nicolas.beziere@med.uni-tuebingen.de
University of Tübingen

**Article**

**Keywords:** Macrophage RAW 264.7, Senescence, Bleomycin, Lipopolysaccharide

**Posted Date:** August 3rd, 2026

**DOI:** https://doi.org/10.21203/rs.3.rs-10316466/v1

**License:** This work is licensed under a Creative Commons Attribution 4.0 International License.
Read Full License

**Additional Declarations:** No competing interests reported.

# Abstract

Macrophage senescence is implicated in age-related immune dysfunction, but *in vitro*models remain limited, in part because the common use of lipopolysaccharide as an inducer also triggers acute inflammatory activation, making it difficult to attribute downstream phenotypes to senescence rather than to M1-type polarisation. Here, we evaluated bleomycin as an alternative senescence inducer in RAW 264.7 murine macrophages and compared it directly to LPS. Bleomycin produced a robust senescent phenotype: 80% senescence-associated beta-galactosidase (SA-β-gal) positivity, ~3-fold p53 protein accumulation with stable Trp53 transcript levels, strong Cdkn1a/p21 upregulation, characteristic morphological changes, and ~80% viability. Ki-67 expression was near-completely abolished, confirming proliferative arrest, with no transcriptional induction of the inflammatory cytokines Il6, Il1a, or Cxcl1 at 48 h. LPS produced the inverse: no SA-β-gal induction, no p21 upregulation, significant Trp53 downregulation, high nitric oxide and ROS output, massive upregulation of Il-6, IL-1α, and CXCL1, and viability below 30%. These findings identify bleomycin as a reliable inducer of macrophage senescence that is cleanly separable from inflammatory activation, and show that the two programs diverge not only on senescence markers but also on inflammatory gene transcription. This model provides a tractable system for studying the cell-autonomous consequences of the senescent state in macrophages independently of the confounding M1 response.


# Introduction

Cellular senescence is a state of robust cell cycle arrest in metabolically active cells [1] that plays a dual role in physiology and pathology. On one hand, it protects against cellular stress and supports tissue homeostasis [2–4]; on the other hand, excessive or dysregulated senescence drives chronic inflammation and tissue dysfunction. The accumulation of senescent cells is a hallmark of aging and contributes to skeletal, neurodegenerative, and metabolic diseases [5–7].

Immunosenescence can be considered a specialized branch of cellular senescence that specifically affects immune cells, leading to age-associated changes in immune structure and function [8]. Senescent immune cells exhibit key characteristics common to all senescent cells, such as irreversible cell cycle arrest and a decline in cellular function [9]. Macrophages, as central components of the innate immune system, can disrupt immune balance and contribute to systemic dysfunction when dysregulated or undergoing senescence [10]. Given their frontline role in immune defense and frequent interactions with senescent cells, macrophages are themselves likely to undergo senescence under specific conditions [11]. Establishing reliable and reproducible models of macrophage senescence is therefore of critical importance. However, before establishing any immunosenescence model, it is important to consider the fine line between immunosenescence and inflammaging — the chronic, low-grade inflammation that develops progressively with age and contributes to many age-related diseases [12]. Fulop et al. described them as two sides of the same coin, meaning that although they cannot be entirely separated, they largely originate from the same underlying processes [13]. In macrophages, LPS is commonly used to

induce inflammatory responses, but has also been used as a senescence inducer for these cells [14–16], raising the question of whether this approach can reliably separate senescence from inflammatory activation. Currently, a standardized model that separates senescence from inflammatory activation is lacking, which limits mechanistic studies and therapeutic targeting. This study aims to clarify their distinction in macrophage biology and to introduce a reproducible model for reliable induction of senescence in macrophages.

Bleomycin, a glycopeptide antibiotic originally isolated from *Streptomyces verticillus*, is widely used to induce senescence in various cell types, including alveolar epithelial cells [17], myoblasts [18], and fibroblasts [19]. It generates DNA double-strand breaks through iron-dependent radical chemistry, triggering the DNA damage response (DDR). The resulting activation of the ATM/ATR kinase cascade leads to post-translational stabilisation of p53, which in turn drives transcription of Cdkn1a/p21 and enforces a stable cell-cycle arrest [1]. This p53–p21 axis is the most consistently reported pathway in bleomycin-induced senescence across cell types, although $p16^{INK4a}$ can also contribute depending on cell lineage and exposure duration [18]. Alongside molecular markers, senescence-associated β-galactosidase (SA-β-gal) activity — reflecting increased lysosomal content — is one of the most widely used cytochemical readouts for identifying senescent cells [1] and serves as a primary endpoint in this study. Notably, the effects of bleomycin are dose-dependent, with a narrow window separating senescence from apoptotic outcomes [20]. This makes careful dose optimisation essential. To our knowledge, bleomycin has not been systematically characterised as a senescence inducer in macrophages.

Here, we evaluate bleomycin as a senescence inducer in RAW264.7 murine macrophages and compare it directly to LPS under parallel conditions. Using a panel of senescence markers (SA-β-gal, p21, p53), gene expression analysis (Trp53, Cdkn1a), and inflammatory and metabolic readouts (NO, ROS, ATP, viability), we test whether bleomycin produces a senescent phenotype that is cleanly separable from the M1-type inflammatory activation induced by LPS.

# Results

### 1 μg/mL bleomycin for 48 hours Effectively Induces β-galactosidase expression in RAW 264.7 Macrophages

Preliminary dose–response testing (0, 0.5, 1, 1.5 and 2 μg/mL) identified 1 μg/mL bleomycin as an optimal concentration for inducing morphological changes indicative of cellular senescence in all independent replicates (Supplementary Data). The experimental design is shown in Fig. 1A. X-gal staining revealed a significant increase in β-gal expression following bleomycin treatment (Fig. 1B). The percentage of X-gal-positive cells increased over time: at 24 h, 9.8 ± 5.5% of cells were X-gal-positive (ns vs. control, 1.2 ± 1.1%). At 48 h, this increased to 80.1 ± 4.3% (****$p < 0.0001$ vs. control), and at 72 h, 78.5 ± 15.5% of cells were X-gal-positive (****$p < 0.0001$ vs. control) (mean ± SD, n = 3 biological

replicates, Fig. 1C). Cells treated with bleomycin for 72 h also displayed morphological features suggestive of apoptosis, including cell shrinkage, membrane blebbing, and formation of apoptotic bodies (Fig. 1B). Based on these findings, the 48 h bleomycin treatment was selected for subsequent experiments.

# Bleomycin and LPS Induce Distinct Morphological Changes in RAW 264.7 Cells

Having established the optimal bleomycin concentration and exposure time, we next compared the cellular responses induced by bleomycin and LPS. The experimental workflow is shown in Fig. 1D. Brightfield microscopy revealed distinct morphological changes in RAW 264.7 macrophages following treatment with 1 μg/mL bleomycin for 48 h or 1 μg/mL LPS for 24 h (Fig. 1E). Compared with untreated controls, both treatments increased cell size but produced different morphologies. Bleomycin-treated cells appeared enlarged with an elongated, irregular morphology, suggestive of a senescence-associated phenotype. In contrast, LPS-treated cells lost their characteristic appearance and adopted a larger, more spread morphology with fewer cellular projections and prominent cytoplasmic vacuolization, consistent with acute macrophage activation and cellular stress.

These morphological differences were further examined by phalloidin staining of F-actin (Fig. 2A). Control cells displayed a compact, round morphology with thin cytoplasmic extensions and well-defined cortical actin. LPS treatment induced pronounced cytoskeletal remodeling, resulting in large, flattened cells with irregular borders, characteristic of activated macrophages. Quantification confirmed a marked increase in cell area compared with controls (Fig. 2B). Bleomycin-treated cells also exhibited a significant increase in cell area but to a lesser extent and a more heterogeneous distribution than LPS-treated cells. Rather than the extensive spreading observed following LPS stimulation, bleomycin-treated cells displayed enlarged, flattened, and irregular cell bodies, features consistent with a senescence-associated phenotype.

## Beta-Galactosidase Staining Reveals Elevated Senescence in bleomycin-Treated Cells Compared to LPS

X-gal staining revealed markedly different results among experimental groups. The bleomycin-treated group exhibited a significantly higher proportion of SA-β-Gal–positive cells (94.2 ± 14.4%, ****$p < 0.0001$ vs. control 1.3 ± 1.7%), with intense blue staining indicating robust induction of senescence. In contrast, the LPS-treated group showed no significant difference compared with the control (1.1 ± 1.9%, ns), suggesting that LPS did not induce a senescent phenotype under these conditions. Baseline β-Gal activity in control cells remained minimal (Fig. 1E,F).

## Ki-67 expression is strongly reduced in bleomycin-treated cells, showing proliferative arrest

To directly assess proliferative status, Ki-67 fluorescence intensity was quantified in all three conditions. Control cells showed abundant Ki-67 expression with strong nuclear staining (Fig. 2C). Both LPS- and bleomycin-treated cells showed reduced Ki-67 signal compared with control ($p < 0.0001$ for both). However, bleomycin-treated cells showed significantly lower Ki-67 intensity than LPS-treated cells ($p < 0.0001$; Fig. 2D) and uniformly low Ki-67 signal, consistent with population-wide cell-cycle arrest, whereas LPS-treated cells showed a heterogeneous reduction with residual Ki-67-positive cells persisting among the surviving fraction.

**Figure 2. Morphological changes and proliferative activity in RAW 264.7 macrophages following bleomycin and LPS treatment. A.** Representative fluorescence images showing DAPI (nuclear staining, blue) and phalloidin (F-actin/cytoskeletal staining, orange) in control, LPS-, and bleomycin-treated cells. Scale bar = 50 μm. **B** Quantification of cell area (μm²) based on phalloidin staining. Both LPS and bleomycin treatment significantly increased cell area compared to control, with LPS-treated cells showing the largest cell area among all groups. **C.** Representative fluorescence images showing DAPI (blue) and Ki-67 (proliferation marker, magenta) staining in control, LPS-, and bleomycin-treated cells. Scale bar = 50 μm. **D.** Quantification of Ki-67 integrated signal density ($10^6$ AU). Both LPS and bleomycin treatment significantly reduced Ki-67 fluorescence intensity compared to control, indicating decreased proliferative activity. Data are presented as violin plots with median (dashed line) and interquartile ranges (dotted lines). Statistical significance was determined by one-way ANOVA/Kruskal-Wallis test; ****$p < 0.0001$

## Bleomycin Treatment Induces Upregulation of p21 and p53 at 48 hours

To complement the cytochemical evidence from SA-β-gal, we examined whether these treatments affected protein expression of senescence-associated markers by immunofluorescence. Analysis of bleomycin- and LPS-treated cells revealed significantly elevated p21 expression in the bleomycin-treated group compared with both the control and LPS-treated groups (Bleomycin: 4.51 ± 3.2; Control: 0.88 ± 0.19, ****$p < 0.0001$; LPS: 0.93 ± 0.25, ****$p < 0.0001$) (Fig. 3A, B). Similarly, p53 staining showed a comparable pattern among the groups, with increased expression in the bleomycin-treated group relative to the control and LPS-treated groups (Bleomycin: 1.40 ± 0.8; Control: 0.52 ± 0.26, ****$p < 0.0001$; LPS: 0.69 ± 0.36, ****$p < 0.0001$, Fig. 3C). However, the staining intensity of p53 was substantially lower than that of p21 (Fig. 3D).

## Bleomycin Treatment Induces Stronger Upregulation of Trp53 and Cdkn1a than LPS at the Gene Level

To compare senescence marker expression between bleomycin and LPS at the transcriptional level, Trp53 and Cdkn1a were assessed by qPCR in both treatment groups. No significant change in Trp53 expression was observed in the bleomycin group compared with the control group (bleomycin: 93% ± 5.3

of control). Surprisingly, Trp53 expression was significantly reduced in the LPS group relative to controls (35.7 ± 8.4%, ****p < 0.0001, Fig. 4A). Cdkn1a expression in the LPS group was not significantly different from controls (LPS: 85.7 ± 6.1% of control) but was significantly higher in the bleomycin group relative to control (bleomycin: 262.7 ± 30.2%, ****p < 0.0001, Fig. 4B).

# Bleomycin Treatment Induces Stronger Upregulation of p21 and p53 Than LPS at the Protein level

Following the analysis of Trp53 and Cdkn1a expression at the gene level, we next examined whether these treatments affected protein expression. Western blot analysis demonstrated a significant increase in p53 and p21 protein levels in the bleomycin-treated group. p53 and p21 protein expression was significantly upregulated in the bleomycin group compared with the control group ($p < 0.01$). In contrast, consistent with the gene-level findings, the LPS-treated group showed no significant change in p53 or p21 protein expression compared with controls ($p > 0.05$, ns) (Fig. 4C, D).

## Cellular stress signatures of LPS- and bleomycin-treated RAW 264.7 cells markedly differ

Having established that bleomycin and LPS diverge on the core senescence markers, we next assessed whether the two treatments also differ in their inflammatory and metabolic profiles. Cell viability decreased to below 30% following treatment with 1 μg/mL LPS for 24 h compared with the control group (Control: 93.6 ± 3.4%; LPS: 27.1 ± 11.4, ****p < 0.0001). In contrast, bleomycin treatment for 48h caused only negligible cytotoxicity, with viability maintained at approximately 80% (78.2 ± 8.8%, *p < 0.05 vs. control) (Fig. 5). Metabolic activity changes were measured by intracellular ATP levels in all groups. ATP levels decreased significantly in both LPS- and bleomycin-treated cells compared with the control group (Control: 1 ± 0.09%; LPS: 0.49 ± 0.05%, ****p < 0.0001; bleomycin: 0.22 ± 0.04%, ****p < 0.0001). Furthermore, ATP levels in the bleomycin group were significantly lower than those in the LPS group, representing an approximately 2.7-fold decrease (****p < 0.0001) (Fig. 5B). To quantify the inflammatory effect of LPS and bleomycin on RAW 264.7 cells, nitrite ($NO_2^-$) levels were measured. LPS treatment significantly increased nitrite levels compared with the control group (Control: 0 ± 0.02%; LPS: 1.25 ± 0.03%, ****p < 0.0001), whereas no significant change was observed in the bleomycin-treated group (bleomycin: 0.02 ± 0.002%, ns) (Fig. 5C). ROS production was altered in treated RAW 264.7 cells. Compared with the control group, LPS treatment significantly increased ROS levels (Control: 1 ± 0.17%; LPS: 1.34 ± 0.33%, **p < 0.01 vs. control), whereas bleomycin treatment significantly decreased ROS production (bleomycin: 0.50 ± 0.14%, ****p < 0.0001 vs. control). ROS levels in the bleomycin-treated group were also significantly lower than those in the LPS-treated group (****p < 0.0001) (Fig. 5D).

**LPS Treatment Induces Upregulation of Pro-Inflammatory Factors IL-6, IL-1α, and CXCL1 Compared with Control and Bleomycin Groups**

Following the assessment of $NO_2^-$ production as an indicator of inflammatory activation, we next evaluated the expression of the pro-inflammatory genes IL-6, IL-1α, and CXCL1 by qPCR. LPS treatment significantly upregulated IL-6 expression compared with the control group (455.1 ± 4.8 fold; ****p < 0.0001). Similarly, IL-1α expression was markedly increased in the LPS group (10,661 ± 85.13 fold; ****p < 0.0001), as was CXCL1 expression (24.06 ± 2.54 fold; ****p < 0.0001), confirming a robust inflammatory response. In contrast, bleomycin-treated cells showed no significant changes in IL-6, IL-1α, or CXCL1 expression relative to controls (Fig. 4E–G).

# Discussion

The aim of this study was to establish whether bleomycin can induce a clean senescent phenotype in RAW264.7 macrophages, and whether it offers a more reliable alternative to LPS for this purpose. Our data indicate that it does, on both counts. The question is not purely methodological: prior work has described LPS itself as a macrophage senescence inducer, blurring the line between inflammatory activation and senescence in ways that complicate any mechanistic reading of macrophage contributions to aging and chronic disease [11].

The effect of bleomycin as a DNA disrupter is mechanistically well-characterised and drives sustained p21 expression and a stable cell-cycle arrest that matures into senescence, a sequence documented in epithelial cells [17], fibroblasts [19], and myoblasts [18], where p21 is the most consistent molecular readout across cell types. To our knowledge, bleomycin has not previously been characterised as a senescence inducer in macrophages. In bleomycin-treated RAW264.7 cells, Trp53 transcript levels remained stable while p53 protein accumulated ~ 3-fold and p21 protein and Cdkn1a transcript were strongly upregulated. This combination — unchanged mRNA and increased protein — is the signature of post-translational p53 stabilisation driven by ATM/DDR signalling [1,21,22], which in turn drives Cdkn1a transcription and the p21-mediated arrest defining the senescent phenotype.

LPS has been reported to induce features of senescence in macrophages across several systems — THP-1 and peritoneal cells [14], vascular calcification models [15], atherosclerosis contexts [16], and most recently a direct LPS vs $H_2O_2$ comparison in peritoneal macrophages and RAW264.7 cells [23]. Our findings diverge from these reports in two aspects. First, under parallel conditions we detect neither Cdkn1a/p21 upregulation nor an increase in SA-β-gal staining above control, while the same cells showed robust M1-type activation. Second, Trp53 expression in LPS-treated cells was significantly reduced rather than elevated, consistent with work showing LPS can downregulate p53 via NF-κB-driven MDM2 activation [24–26]. Notably, Danish et al. themselves observed that the senescence-marker response in RAW264.7 was weaker than in primary peritoneal cells and recommended the latter for senescence modelling. In RAW264.7 under acute exposure, LPS produces inflammatory activation without the core cell-autonomous senescence hallmarks, and is therefore better used as a reference point for M1 activation than as a stand-alone senescence inducer.

The qPCR data on Il-6, IL-1α, and CXCL1 reinforce the separation between the two programs at the level of inflammatory gene transcription. LPS-treated cells showed massive upregulation of all three genes, consistent with canonical TLR4/NF-κB-driven inflammatory transcription, contrary to bleomycin-treated cells. While these genes are also core SASP components, growth arrest and SASP are mechanistically parallel programs driven by different branches of the DDR: p53/p21 mediates the arrest, while persistent DDR signalling through ATM and NF-κB drives the secretory phenotype, typically reaching full expression only after five or more days [27,28]. Our 48 h readout captures the cell-autonomous arrest program before the secretory program has engaged, consistent with the timeline reported for bleomycin-induced SASP in epithelial cells [17,29]. The LPS cytokine response, by contrast, reflects acute TLR4/NF-κB activation — the same transcription factor and many of the same targets as SASP, but driven by pathogen recognition rather than persistent DNA damage. This mechanistic overlap is precisely what makes LPS unreliable as a senescence inducer, and what the present model is designed to avoid. Whether bleomycin-induced senescent macrophages develop SASP at later timepoints remains open [30,31] and will require a time-course study to resolve.

Of the readouts in this study, ROS production shows the most unexpected pattern: bleomycin-treated cells showed ROS reduced to ~ 50% of control at 48 h, while LPS-treated cells showed the expected ~ 34% increase. Since DCF-DA does not distinguish mitochondrial from NOX-derived sources, the divergence likely reflects NOX2-mediated respiratory burst under M1 activation rather than a senescence-specific redox shift.

Taken together, these readouts describe two fundamentally different cellular states. The most consequential difference is that at 24 h of LPS exposure, RAW264.7 viability dropped to 27.1 ± 11.4%, compared with ~ 80% for bleomycin at 48 h. Cellular senescence is, by definition, a state of stable, persistent, non-proliferative viability; a population in which three-quarters of cells have died cannot serve as a stable model of that state regardless of which markers the surviving fraction expresses. Bleomycin-treated cells, by contrast, adopt a metabolically subdued but durable state. This observation is reinforced by the low Ki-67 expression. The bleomycin-treated cells showed uniformly low Ki-67 consistent with population-wide arrest, whereas LPS-treated cells retained heterogeneous Ki-67 expression among the surviving fraction, suggesting collateral growth suppression in a dying population rather than coordinated cell-cycle exit. This distinction between durability versus lethality may be the single most useful criterion separating a senescence model from an acute insult in macrophages.

Several limitations should be acknowledged. RAW264.7 is an immortalised line and does not fully recapitulate primary macrophage biology; validation in primary bone marrow-derived and tissue-resident macrophages will be required before the model can be generalised. We profiled three core SASP-associated genes (Il6, Il1α, CXCL1) and found no transcriptional induction at 48 h, but SASP is a late-developing feature of senescence, and a single timepoint cannot determine whether the secretory program engages at later stages. Finally, the ROS measurement cannot distinguish NOX2-derived from mitochondrial sources, a limitation that a source-resolved follow-up should address.

A macrophage senescence model inducible independently of M1 activation opens several lines of investigation, particularly because disentangling senescent macrophage contributions from classical inflammatory activation has been difficult in existing systems[11]. Three directions follow immediately: a SASP time-course extending to 7–14 days to determine whether the secretory program eventually engages, functional assays of phagocytosis and efferocytosis to test whether phagocytic decline reflects senescence or inflammatory activation, and validation in primary macrophages and in vivo models to establish translational relevance. The broader value of the model lies in making macrophage senescence accessible to the experimental logic that has shaped fibroblast and epithelial senescence research .

## Conclusion

We have identified bleomycin as a reliable inducer of cellular senescence in RAW264.7 macrophages, producing the core hallmarks including sustained p21 upregulation, SA-β-gal positivity, near-complete loss of Ki-67 expression, and stable viability without engaging the M1-type inflammatory activation or NF-κB-driven cytokine transcription that accompanies LPS exposure. Under parallel conditions, LPS produced the inverse phenotype: classical inflammatory activation with high NO and ROS output, massive Il6, IL-1α, and CXCL1 upregulation, Trp53 downregulation, no induction of core senescence markers, and substantial loss of viability. These findings provide a tractable in vitro system for studying macrophage senescence independently of inflammatory activation. Validation in primary macrophages, in vivo models, and a full time course SASP characterisation will establish the generality of the model.

## Materials and Methods

# Reagents

Bleomycin sulfate powder (Thermo Fisher Scientific, Cat# J60727) was dissolved in PBS to 1 mg/mL and stored at − 20°C until use. Lipopolysaccharide (LPS; Sigma-Aldrich, Cat# L3129) was resuspended in Phosphate-buffered saline (PBS) to 5 mg/mL and stored at − 20°C.

# Cell Culture

RAW 264.7 macrophage cells (ATCC, Cat# TIB-71) were cultured in complete Dulbecco's Modified Eagle Medium (DMEM) High Glucose with Stable Glutamine and Sodium Pyruvate (Capricorn Scientific, Cat# DMEM-HPSTA) supplemented with 10% fetal bovine serum (FBS; Sigma-Aldrich, Cat# F7524) and 100 U/mL Penicillin-Streptomycin (Pen-Strep; Sigma-Aldrich, Cat# P0781) at 37°C in a humidified incubator with 5% $CO_2$. Cells were used at passage numbers below 5 to avoid replicative senescence.

# Senescence Induction

Before starting the experiment, 1 × $10^6$ RAW 264.7 cells were plated for 24 h in complete medium at 37°C in a 5% $CO_2$ humidified incubator. Subsequently, cells were treated with LPS (1 μg/mL) for 24 h. Bleomycin was then tested at five different doses (0.1, 0.5, 1, 1.5, and 2 μg/mL) for 24 h, 48 h or 72 h.

The optimal bleomycin dose was determined based on Senescence-Associated Beta-Galactosidase staining (SA-β-gal staining) and morphological assessment to identify the concentration that primarily induces senescence without causing significant cell death.

# Senescence-associated β-galactosidase (SA-β-gal) staining

Cells were fixed with 25% glutaraldehyde in $H_2O$ (Sigma-Aldrich, Cat# G5882) and 4% paraformaldehyde in PBS (Thermo Fisher Scientific, Cat# J19943.K2) for 15 min at room temperature, incubated with 5-bromo-4-chloro-3-indolyl β-D-galactopyranoside (X-Gal; Avantor Sciences, Cat# 2994430) at pH 6.0 for 24 h, washed with $MgCl_2$ solution, and imaged at 20× magnification. Cells were plated at $1 \times 10^6$ cells per petri dish. Stained cells (blue) were expressed as a percentage of the total cell number and quantified by manual counting of randomly selected fields using ImageJ software.

# Cell viability

The Trypan Blue (Sigma-Aldrich, CAS 72-57-1) exclusion assay was used to determine cell growth and viability. Briefly, RAW 264.7 cells were trypsinized, stained with Trypan Blue, and the number of live and dead cells was counted using a hemocytometer under a light microscope.

# ATP-based Metabolic Activity Assay

RAW 264.7 cells were seeded at a density of $1 \times 10^5$ cells per well in 96-well plates and incubated for 24 h. LPS and bleomycin treatments were then performed as described above. ATP levels were measured using the CellTiter-Glo Luminescent Cell Viability Assay (Promega, Cat# G7570), following the manufacturer's instructions. Results are expressed as relative light units (RLU), and error bars represent the standard deviation.

# Nitric oxide measurement

The production of nitric oxide (NO) by macrophages was evaluated using the Griess assay as an indicator. 100 µL of culture medium was collected from each well and mixed with 100 µL of Griess reagent (modified) (Sigma-Aldrich, Cat# G4410). The mixture was incubated for 15 min at room temperature in the dark, and absorbance at 550 nm was measured using a microplate reader. Untreated control samples were processed and measured under the same conditions.

# Reactive oxygen species (ROS) measurement

RAW 264.7 cells ($1 \times 10^4$ cells/well) were seeded in a 96-well plate and allowed to adhere for 24 h. Cells were then treated separately with LPS (1µg/mL) or bleomycin (1µg/mL) for 24 h and 48 h, respectively. After treatment, cells were washed twice with PBS and stained with 100 µL/well of DCF-DA solution for 30 min at 37°C in the dark. Following staining, the DCF-DA solution was removed, cells were washed, and 100 µL/well of PBS was added. Fluorescence was measured at an excitation wavelength of 485 nm and emission wavelength of 535 nm using the ROS Detection Kit (OzBiosciences, Cat# ROS0300).

# RNA extraction and quantitative real time PCR

Total RNA was isolated using the peqGOLD RNA Kit (Peqlab, Cat# 27582713) according to the manufacturer's instructions. cDNA synthesis was performed using the High-Capacity cDNA Reverse Transcription Kit (Thermo Fisher Scientific, Cat# 4374966) according to the manufacturer's instructions. Quantitative PCR (qPCR) was carried out in triplicate on a LightCycler® 480 Instrument II. Primer sequences are listed in Table 1. Relative mRNA expression levels were calculated using the $2^{-}\Delta\Delta CT$ method and normalized to GAPDH as the housekeeping gene.

Table 1
Primer sequences used in this study

| Gene | Primer | Sequence (5'–3') |
|---|---|---|
| GAPDH | Forward | ACACATTGGGGGTAGGAACA |
| GAPDH | Reverse | AACTTTGGCATTGTGGAAGG |
| Cdkn1a | Forward | TTG TCG CTG TCT TGC ACT CT |
| Cdkn1a | Reverse | TTT CGG CCC TGA GAT GTT CC |
| Trp53 | Forward | CACAGCGTGGTGGTACCTTA |
| Trp53 | Reverse | TCTTCTGTACGGCGGTCTCT |
| IL-6 | Forward | CACTTCACAAGTCGGAGGCT |
| IL-6 | Reverse | CTGCAAGTGCATCATCGTTGT |
| IL-1α | Forward | ACGAAGACTACAGTTCTGCCA |
| IL-1α | Reverse | GTGCAAGTCTCATGAAGTGAGC |
| Cxcl1 | Forward | ATGGCTGGGATTCACCTCAAG |
| Cxcl1 | Reverse | GAGTGTGGCTATGACTTCGGT |

# Immunostaining

RAW 264.7 cells were seeded in a 96-well plate at a density of $1 \times 10^4$ cells per well. After fixation with 4% paraformaldehyde (PFA) for 15 min, the cells were washed with PBS. Next, a blocking buffer containing 1% bovine serum albumin (BSA) and 0.3% Triton X-100 was applied for 1 h. Subsequently, cells were incubated overnight with either p21 primary antibody (AB188224; Abcam), p53 primary antibody (AB131442; Abcam) or Ki-67 antibody (Miltenyi Biotec, Cat. No. 130-128-745). The following day, the cells were washed and incubated for 2 h with secondary antibodies, including donkey anti-rabbit Alexa Fluor 488 (A32790) and donkey anti-rabbit Alexa Fluor 647 (A31573). F-actin was counterstained

with phalloidin, and nuclei were stained with DAPI. Following additional PBS washes, images were acquired.

# Immunofluorescence image acquisition and analysis

Immunofluorescence images of, p21-, p53- and Ki-67-stained RAW 264.7 cells were acquired using a Leica DMi8 inverted microscope equipped with a THUNDER imaging module (Leica Microsystems, Wetzlar, Germany), a Leica LED3 light source, a Leica K5 camera, and a HC PL FLUOTAR 10×/0.32 Dry objective. DAPI was used for nuclear counterstaining; DAPI, Ki-67, p21, and p53 and Ki-67 were detected using the LED_405 (excitation 375–435 nm, emission 450–490 nm), Y5 (excitation 590–650 nm, emission 662–738 nm), FITC (excitation 460–500 nm, emission 512–542 nm), and Y5 (excitation 590–650 nm, emission 662–738 nm) filters, respectively. Within each experiment, all conditions were imaged using identical acquisition settings, including exposure time, illumination intensity, and gain. Image analysis was performed in Fiji/ImageJ version 1.54p using a custom ImageJ macro. Nuclei were segmented in the DAPI channel using StarDist's internal Versatile (fluorescent nuclei) model [32]. The resulting masks were used directly to quantify the p21 or p53 immunofluorescence signal per nucleus. Integrated fluorescence intensity was measured for each segmented nucleus.

For each condition, n = 3 biological replicates were analyzed, including 4 fields of view per well and > 15,000 total cells per group. Single-cell values were pooled for visualization as violin plots.

# Western blot

Cells were detached using a cell scraper, and total cellular proteins were extracted in RIPA buffer (Thermo Fisher Scientific, Cat# 89901), supplemented with a Protease inhibitor cocktail tablet (Roche, Cat# 04693124001) and Phosphatase inhibitor mini tablets (Thermo Fisher Scientific, Cat# A32957). Protein concentration was determined using the Micro BCA™ Protein Assay Kit (Thermo Fisher Scientific, Cat# 23235). Samples were mixed with 6× loading buffer and denatured at 95°C for 5 min. SDS-PAGE was performed by loading 30 µg of each sample and running at 130 V for 90 min at RT. Blots were blocked with 2.5% non-fat dry milk (Santa Cruz Biotechnology, Cat# SC-2324) in TBST. After incubating with primary antibodies (p21, AB188224; p53, AB131442; Abcam) overnight at 4°C, blots were washed twice with TBST and incubated with secondary antibody IRDye 800CW Donkey Anti-Rabbit secondary antibody (Li-Cor, Cat# 926-32213)) for 1 h at RT. Finally, the blots were washed again and visualized using the Odyssey infrared imaging system. For all Western Blot experiments, quantification was normalized to β-actin loading controls.

# Statistical analysis

Data are presented as the mean ± standard deviation (SD). Differences between two groups were assessed using one-way ANOVA. All statistical analyses were conducted using GraphPad Prism 8.0, and a p-value less than 0.05 was considered statistically significant. All comparison experiments between bleomycin and LPS groups were performed with n = 3 biological replicates unless otherwise stated.

# Declarations

### Use of Large Language Models

AI-assisted writing tools (Claude, Anthropic) were used to assist with manuscript structuring, drafting, and revision. All content was critically reviewed, verified against primary data, and edited by the authors, who take full responsibility for the scientific content and interpretations.


### Acknowledgements

We thank Linda Schramm and Olga Elberg for their technical support, as well as Eden Laing, Sophie Tonneau, Jonathan Cotton and Francisco Reche for the critical scientific discussions. We also acknowledge the Interfaculty Institute of Biochemistry at the Eberhard Karls University of Tübingen for their support. This work was supported by the Werner Siemens Foundation.


### Author Contributions

K.K. performed the experiments, analyzed the data, and wrote the manuscript. O.H. performed image acquisition for the immunofluorescence staining experiments and developed the analysis code. M.B. contributed to cell culture and immunoblotting experiments. B.J.P. provided scientific supervision. B.W. supervised the microscopy work. N.B. supervised the project and contributed to study design. All authors revised, read and approved the manuscript.

### Data availability statement

The data supporting the findings of this study are available from the corresponding author upon reasonable request.

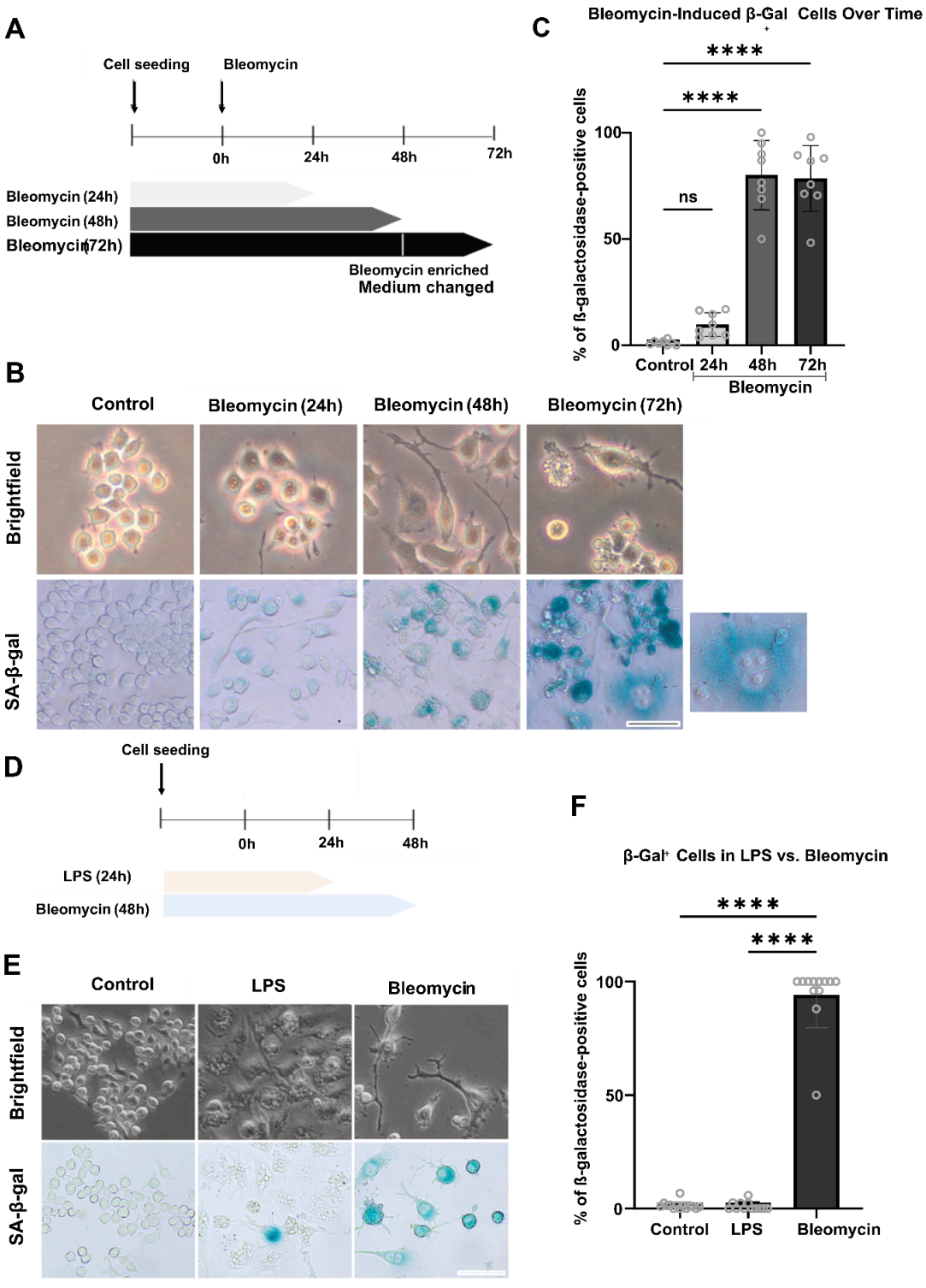
# References


1. Gorgoulis, V. et al. Cellular Senescence: Defining a Path Forward. *Cell* **179**, 813–827. https://doi.org/10.1016/j.cell.2019.10.005 (2019).
2. Dong, Z. et al. Cellular senescence and SASP in tumor progression and therapeutic opportunities. *Mol. Cancer*. **23**, 181. https://doi.org/10.1186/s12943-024-02096-7 (2024).
3. Storer, M. et al. Senescence is a developmental mechanism that contributes to embryonic growth and patterning. *Cell* **155**, 1119–1130. https://doi.org/10.1016/j.cell.2013.10.041 (2013).
4. Demaria, M. et al. An essential role for senescent cells in optimal wound healing through secretion of PDGF-AA. *Dev. Cell.* **31**, 722–733. https://doi.org/10.1016/j.devcel.2014.11.012 (2014).
5. He, X. et al. Cellular senescence in skeletal disease: mechanisms and treatment. *Cell. Mol. Biol. Lett.* **28**, 88. https://doi.org/10.1186/s11658-023-00501-5 (2023).
6. Martinez-Cue, C. & Rueda, N. Cellular Senescence in Neurodegenerative Diseases. *Front. Cell. Neurosci.* **14**, 16. https://doi.org/10.3389/fncel.2020.00016 (2020).

7. Spinelli, R. et al. Increased cell senescence in human metabolic disorders. *J. Clin. Invest.* **133** https://doi.org/10.1172/JCI169922 (2023).
8. Ayoub, M., Abou Jaoude, C., Ayoub, M., Hamade, A. & Rima, M. The Immune System and Cellular Senescence: A Complex Interplay in Aging and Disease. *Immunology* **177**, 149–169. https://doi.org/10.1111/imm.70036 (2026).
9. Wang, S. et al. Recent Advances in Aging and Immunosenescence: Mechanisms and Therapeutic Strategies. *Cells* **14**, 499. https://doi.org/10.3390/cells14070499 (2025).
10. Jackaman, C. et al. Aging and cancer: The role of macrophages and neutrophils. *Ageing Res. Rev.* **36**, 105–116. https://doi.org/10.1016/j.arr.2017.03.008 (2017).
11. Behmoaras, J. & Gil, J. Similarities and interplay between senescent cells and macrophages. *J. Cell. Biol.* **220**, e202010162. https://doi.org/10.1083/jcb.202010162 (2021).
12. Garcia-Dominguez, M. Pathological and Inflammatory Consequences of Aging. *Biomolecules* **15**, 404. https://doi.org/10.3390/biom15030404 (2025).
13. Fulop, T. et al. Immunosenescence and Inflamm-Aging As Two Sides of the Same Coin: Friends or Foes? *Front. Immunol.* **8**, 1960. https://doi.org/10.3389/fimmu.2017.01960 (2017).
14. Wang, H. et al. BRD4 contributes to LPS-induced macrophage senescence and promotes progression of atherosclerosis-associated lipid uptake. *Aging (Albany NY)*. **12**, 9240–9259. https://doi.org/10.18632/aging.103200 (2020).
15. Fang, Y. P. et al. LPS-induced senescence of macrophages aggravates calcification and senescence of vascular smooth muscle cells via IFITM3. *Ren. Fail.* **46**, 2367708. https://doi.org/10.1080/0886022X.2024.2367708 (2024).
16. Suzuki, K., Susaki, E. A. & Nagaoka, I. Lipopolysaccharides and Cellular Senescence: Involvement in Atherosclerosis. *Int. J. Mol. Sci.* **23**, 11148. https://doi.org/10.3390/ijms231911148 (2022).
17. Chen, F. et al. Bleomycin induces senescence and repression of DNA repair via downregulation of Rad51. *Mol. Med.* **30**, 54. https://doi.org/10.1186/s10020-024-00821-y (2024).
18. Kamal, M., Joanisse, S. & Parise, G. Bleomycin-treated myoblasts undergo p21-associated cellular senescence and have severely impaired differentiation. *Geroscience* **46**, 1843–1859. https://doi.org/10.1007/s11357-023-00929-9 (2024).
19. Lim, H., Park, H. & Kim, H. P. Effects of flavonoids on senescence-associated secretory phenotype formation from bleomycin-induced senescence in BJ fibroblasts. *Biochem. Pharmacol.* **96**, 337–348. https://doi.org/10.1016/j.bcp.2015.06.013 (2015).
20. Linge, A., Weinhold, K., Blasche, R., Kasper, M. & Barth, K. Downregulation of caveolin-1 affects bleomycin-induced growth arrest and cellular senescence in A549 cells. *Int. J. Biochem. Cell. Biol.* **39**, 1964–1974. https://doi.org/10.1016/j.biocel.2007.05.018 (2007).
21. d'Adda di Fagagna. A DNA damage checkpoint response in telomere-initiated senescence. *Nature* **426**, 194–198. https://doi.org/10.1038/nature02118 (2003).

22. Bartkova, J. et al. Oncogene-induced senescence is part of the tumorigenesis barrier imposed by DNA damage checkpoints. *Nature* **444**, 633–637. https://doi.org/10.1038/nature05268 (2006).
23. Danish, M. et al. Comparative evaluation of cellular senescence in naturally aged and stress-induced murine macrophages for identifying optimum senescent macrophage study systems. *Mol. Biol. Rep.* **52**, 123. https://doi.org/10.1007/s11033-025-10232-9 (2025).
24. Brighenti, E. et al. Interleukin 6 downregulates p53 expression and activity by stimulating ribosome biogenesis: a new pathway connecting inflammation to cancer. *Oncogene* **33**, 4396–4406. https://doi.org/10.1038/onc.2014.1 (2014).
25. Zhang, T. et al. p53 predominantly regulates IL-6 production and suppresses synovial inflammation in fibroblast-like synoviocytes and adjuvant-induced arthritis. *Arthritis Res. Ther.* **18**, 271. https://doi.org/10.1186/s13075-016-1161-4 (2016).
26. Odkhuu, E. et al. Lipopolysaccharide downregulates the expression of p53 through activation of MDM2 and enhances activation of nuclear factor-kappa B. *Immunobiology* **220**, 136–141. https://doi.org/10.1016/j.imbio.2014.08.010 (2015).
27. Coppe, J. P. et al. Senescence-associated secretory phenotypes reveal cell-nonautonomous functions of oncogenic RAS and the p53 tumor suppressor. *PLoS Biol.* **6**, 2853–2868. https://doi.org/10.1371/journal.pbio.0060301 (2008).
28. Rodier, F. et al. Persistent DNA damage signalling triggers senescence-associated inflammatory cytokine secretion. *Nat. Cell. Biol.* **11**, 973–979. https://doi.org/10.1038/ncb1909 (2009).
29. Spina, J. S. et al. Modulating in vitro lung fibroblast activation via senolysis of senescent human alveolar epithelial cells. *Aging (Albany NY)*. **16**, 10694–10723. https://doi.org/10.18632/aging.205994 (2024).
30. Coppe, J. P., Desprez, P. Y., Krtolica, A. & Campisi, J. The senescence-associated secretory phenotype: the dark side of tumor suppression. *Annu. Rev. Pathol.* **5**, 99–118. https://doi.org/10.1146/annurev-pathol-121808-102144 (2010).
31. Wang, B. et al. Pharmacological CDK4/6 inhibition reveals a p53-dependent senescent state with restricted toxicity. *EMBO J.* **41**, e108946. https://doi.org/10.15252/embj.2021108946 (2022).
32. Schmidt, U., Weigert, M., Broaddus, C. & Myers, G. in *International conference on medical image computing and computer-assisted intervention.* 265–273 (Springer) https://doi.org/10.1007/978-3-030-00934-2_30

# Figures




## Figure 1

**Senescence induction in RAW 264.7 cells. A.** Experimental workflow of bleomycin treatments at different time points. **B.** Morphology and SA-β-galactosidase activity in RAW 264.7 cells. Untreated control cells (left) are shown alongside cells treated with 1 µg/mL bleomycin for 24, 48, and 72 h. **C.** Quantification of SA-β-galactosidase activity in RAW 264.7 cells following bleomycin treatment Bleomycin 24 h, 48 h, 72 h compared with control. **D.** Experimental scheme of bleomycin (1 µg/mL, 48 h)

and LPS (1 µg/mL, 24 h) treatments in RAW 264.7 cells **E.** Comparison of morphology and SA-β-galactosidase activity following treatment with bleomycin and LPS. **F.** Quantification of SA-β-galactosidase activity following bleomycin and LPS treatments. Data were analyzed using ordinary one-way ANOVA (****p < 0.0001). Scale bar = 50 µm.

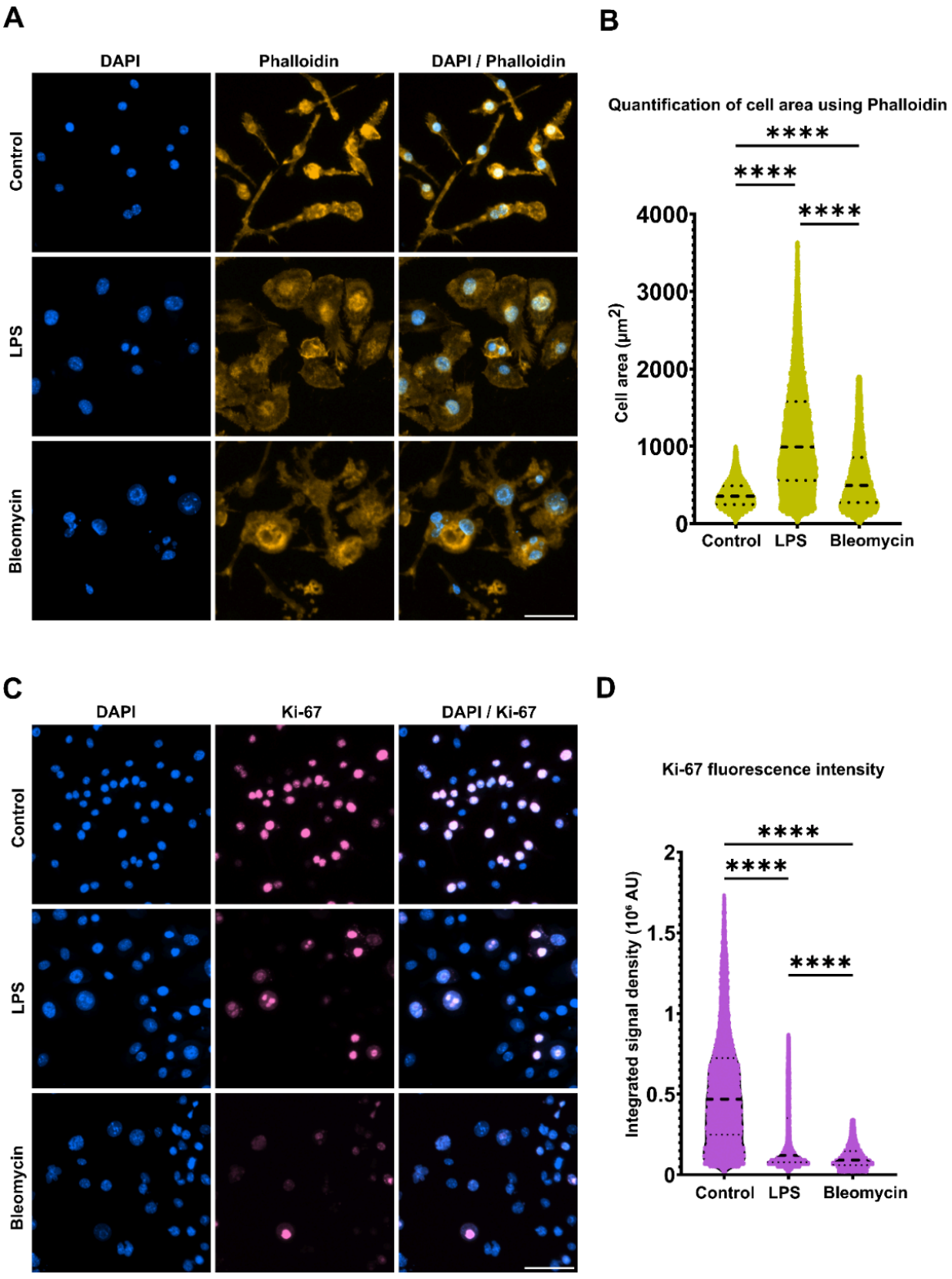



**Figure 2**

**Morphological changes and proliferative activity in RAW 264.7 macrophages following bleomycin and LPS treatment. A.** Representative fluorescence images showing DAPI (nuclear staining, blue) and phalloidin (F-actin/cytoskeletal staining, orange) in control, LPS-, and bleomycin-treated cells. Scale bar = 50 μm. **B**Quantification of cell area (μm²) based on phalloidin staining. Both LPS and bleomycin treatment significantly increased cell area compared to control, with LPS-treated cells showing the largest cell area among all groups. **C.**Representative fluorescence images showing DAPI (blue) and Ki-67 (proliferation marker, magenta) staining in control, LPS-, and bleomycin-treated cells. Scale bar = 50 μm. **D.** Quantification of Ki-67 integrated signal density ($10^6$ AU). Both LPS and bleomycin treatment significantly reduced Ki-67 fluorescence intensity compared to control, indicating decreased proliferative activity. Data are presented as violin plots with median (dashed line) and interquartile ranges (dotted lines). Statistical significance was determined by one-way ANOVA/Kruskal-Wallis test; ****$p < 0.0001$

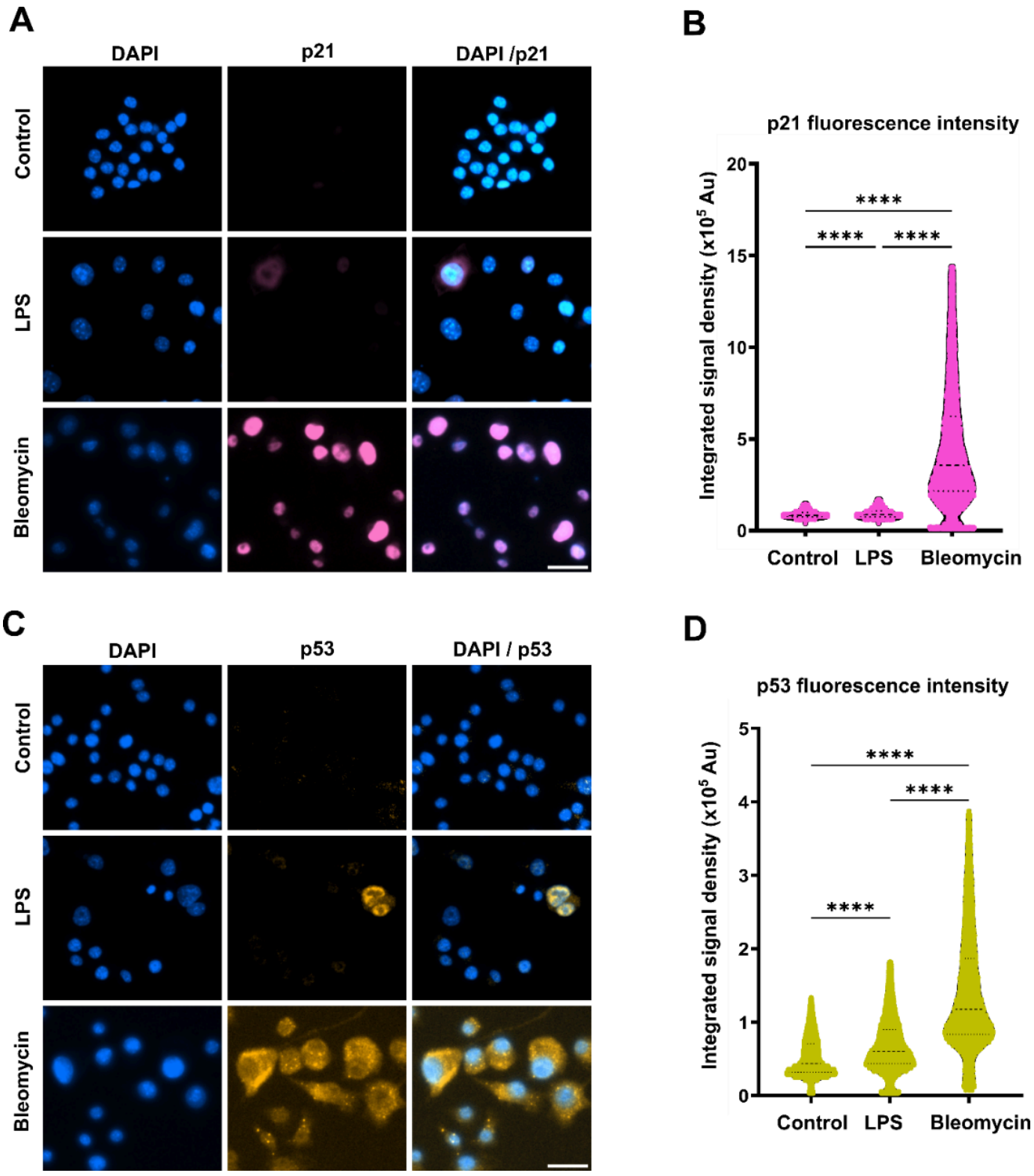



Figure 3

**Single-cell immunofluorescence analysis of p21 and p53 in RAW 264.7 cells. (A, C) Representative** immunofluorescence images of RAW 264.7 cells stained for p21 (magenta) or p53 (yellow) after treatment with bleomycin or LPS. Nuclei were counterstained with DAPI (blue). The top row shows untreated control cells, the middle row shows LPS-treated cells, and the bottom row shows bleomycin-treated cells. **(B, D)** Single-cell quantification of p21 (B) and p53 (D) immunofluorescence signal, shown

as background-corrected integrated fluorescence intensity per segmented cell. Violin plots show pooled single-cell measurements from n = 3 biological replicates ( >18.10$^3$ cells per group). Statistical analysis was performed using Kruskal-Wallis test on pooled single-cell values. Significance levels are indicated as **** p < 0.0001. Scale bar = 50 µm.

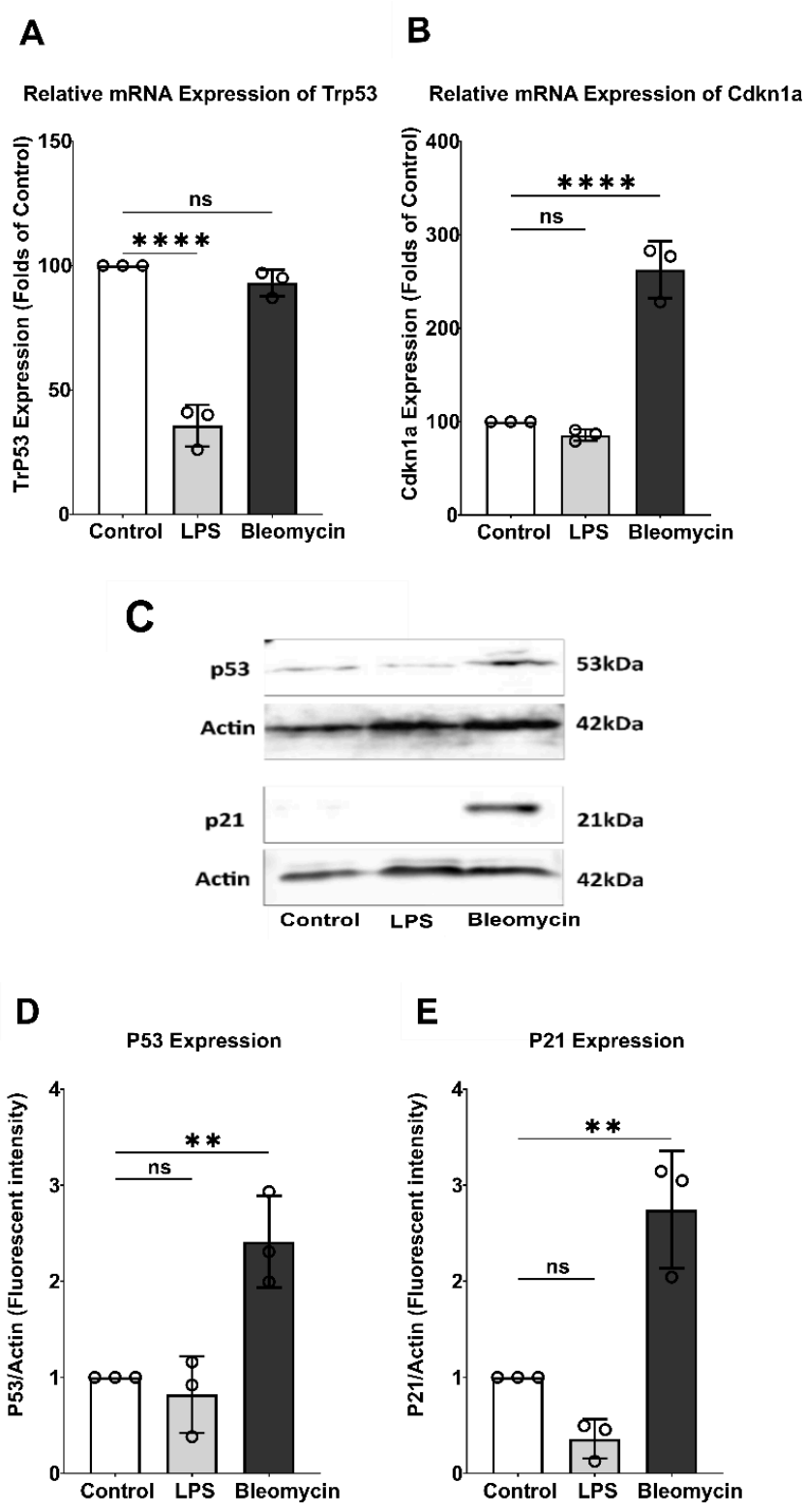
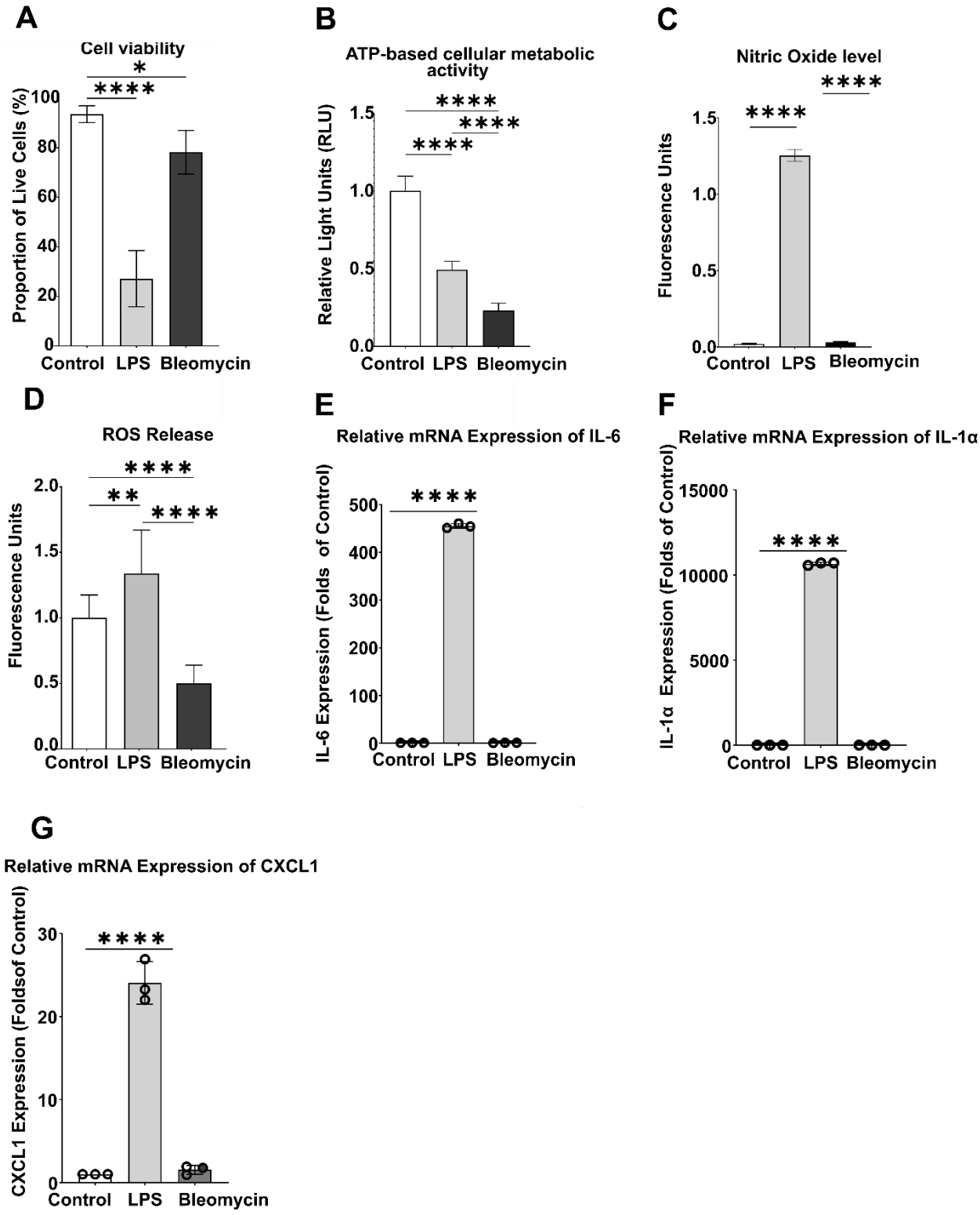



**Figure 4**

**Quantification of the expression of senescence associated proteins A**. Relative mRNA levels of TrP53 measured by qPCR and **B.** corresponding Cdkn1a expression. TrP53 mRNA levels did not change significantly in the BLM group compared with control, whereas the LPS group showed a significant downregulation ($P < 0.0001$). Expression of CDKN1A was significantly upregulated in the BLM group but remained unchanged in the LPS group. **C–E. Western blot analysis of p53 and p21 protein levels.** Quantification normalized to β-actin loading controls revealed significant increases in both proteins in the BLM group ($p < 0.01$) compared with controls, whereas no significant changes were observed in the LPS group.




## Figure 5

**Inflammatory responses of RAW 264.7 cells to LPS and bleomycin**. **A.** Cell viability: LPS markedly reduced cell viability compared with control (****p < 0.0001), whereas bleomycin caused a moderate reduction (*p < 0.05). **B**. ATP Assay: Both LPS and bleomycin treatments decreased ATP levels (Control vs. LPS ****p < 0.0001; Control vs. bleomycin ****p < 0.0001). **C.** LPS strongly elevated $NO_2^-$ (****p < 0.0001), while bleomycin did not significantly alter $NO_2^-$ levels. **D.** Reactive oxygen species (ROS) activity:

LPS increased ROS levels (**p < 0.01), whereas bleomycin decreased ROS by roughly 50% compared with control (****p < 0.0001). Data were analyzed using ordinary one-way ANOVA. **E**. Relative mRNA expression levels of IL-6 measured by qPCR, **F.**corresponding IL-1α expression, and **G.** CXCL1 expression. IL-6, IL-1α , and CXCL1 were significantly upregulated in the LPS-treated group compared with the control group (****p < 0.0001), whereas the bleomycin-treated group showed no significant changes.

## Supplementary Files

This is a list of supplementary files associated with this preprint. Click to download.

- SuppMat.pdf